Eur Biophys J (2009) 38:911–922
DOI 10.1007/s00249-009-0471-8

ORIGINAL PAPER

Methods and estimations of uncertainties in single-molecule dynamic force spectroscopy

Oscar Björnham · Staffan Schedin

Received: 28 January 2009 / Revised: 20 April 2009 / Accepted: 28 April 2009 / Published online: 22 May 2009

Abstract In dynamic force spectroscopy, access to the characteristic parameters of single molecular bonds requires nontrivial measurements and data processing as the rupture forces are found not only to be distributed over a wide range, but are also dependent on the loading rate. The choice of measurement procedure and data processing methods has a considerable impact on the accuracy and precision of the final results. We analyze, by means of numerical simulations, methods to minimize and assess the magnitude of the expected errors for different combinations of experimental and evaluation methods. It was found that the choice of fitting function is crucial to extract correct parameter values. Applying a Gaussian function, which is a common practice, is equivalent to introducing a systematic error, and leads to a consequent overestimation of the thermal off-rate by more than 30%. We found that the precision of the bond length and the thermal off-rate, in presence of unbiased noise, were improved by reducing the number of loading rates for a given number of measurements. Finally, the results suggest that the minimum number of measurements needed to obtain the bond strength, with acceptable precision, exceeds the common number of ~ 100 reported in literature.

Keywords Specific binding · DFS · Receptor–ligand · Error propagation · Bond length · Thermal off-rate · Monte Carlo simulation

O. Björnham · S. Schedin (✉)
Department of Applied Physics and Electronics,
Umeå University, 901 87 Umeå, Sweden
e-mail: Staffan.Schedin@tfe.umu.se

Nomenclature

Bond strength	Most probable rupture force
Accuracy	A measure of the correctness of the mean value of a data set
Precision	A measure of the spread of values of a set of data
RPDD	Rupture probability density distribution
KDE	Kernel density estimation
SD	Standard deviation
True bond strength	The intrinsic bond strength of the bond
True thermal off-rate	The intrinsic thermal off-rate of the bond

Introduction

Dynamic force spectroscopy (DFS) has become a common and powerful tool for investigation of the intrinsic properties of single specific molecular bindings in biological systems, such as receptor–ligand bindings. In DFS, a gradually increasing tensile force is applied to a bonded molecular pair, and the rupture force, when the molecular bond is dissociated, is measured. Different experimental techniques are available to separate single specific molecular complexes, of which biomembrane force probes (Chen et al. 2008; Merkel et al. 1999; Perret et al. 2004), atomic force microscopy (Fuhrmann et al. 2008; Lee et al. 2007; Marshall et al. 2005; Odorico et al. 2007a; Zhang et al. 2004), and optical tweezers (Arya et al. 2005; Bianco et al. 2007; Björnham et al. 2009) are the most commonly used. The theoretical foundation of DFS (Evans and Ritchie 1997) is based on the original kinetic transition theory (Bell

1978; Kramers 1940). The basic concept is that a molecular binding experiences an exponentially increasing off-rate when it is exposed to an external force. By increasing the external force linearly with time (i.e., constant loading rate) the binding is compelled to rupture within a sufficiently short time interval with respect to the experimental time scale. The minute force, often in the lower piconewton range, at which the binding ruptures, is recorded and by repeating the rupture experiment a large number of times with the same loading rate, a frequency distribution of rupture forces is obtained. A fitting procedure applied to the force distribution provides a maximum frequency at a certain force, which is defined as the most probable rupture force or the bond strength of the bond, at the present loading rate. It is a common practice in the literature to use a Gaussian as a fitting function despite the fact that the expected rupture force distribution is not Gaussian (Bartels et al. 2007; Odorico et al. 2007b; Rico and Moy 2007; Strunz et al. 1999). The influence of this discrepancy is quantitatively investigated in detail in this study. Based on kinetic transition theory, the bond strength depends linearly on the logarithm of the loading rate. From this linear relationship, information about the bond length and the thermal off-rate, which are in general the two parameters of greatest interest in DFS studies, can be explicitly derived. These parameters can be used to describe the basic structure of the energy landscape of the molecular bond. This procedure, applicable to so-called slip bonds, has been practiced frequently in recent years (Berquand et al. 2005; Björnham et al. 2009; Derenyi et al. 2004; Evans and Ritchie 1997; Neuert et al. 2006; Schwesinger et al. 2000; Yuan et al. 2000).

The lifetime of a molecular bond is governed by stochastic thermal processes, which means that a single measurement returns a rupture force that is a random sample from a probability distribution. This distribution has a variance that is reflected in the spread of the measured rupture forces. It has been assumed, in general, that at least $\sim$100 measurements are needed to obtain the bond strength with acceptable precision (Evans 1999; Merkel et al. 1999; Touhami et al. 2007; Williams 2003). This work is dedicated to analyze, by means of numerical simulations, the magnitude of the expected errors in the resulting parameters of a DFS analysis (the bond strength, bond length, and off-rate) depending on the noise in the system, but also the choice of measurement procedure, i.e., the number of loading rates at which measurements are performed. In addition, examination of different data processing methods and their impact on the accuracy and precision of the results are conducted. These methods include histogram representations and curve-fitting methods. The simulations are based on simulations of single-state transitions. The results can be applied even for more complex bonds, with several intermediate transition states, since the analysis procedure for each state is the same as for a single state. This analysis serves as a guide to experimenters performing unbinding experiments of single molecular bonds with DFS.

Theory

This work is based on the original bond kinetics theory (Bell 1978), which was later refined (Evans and Ritchie 1997), and is exclusively dedicated to the common loading case with a linearly increasing external force, i.e., constant loading rate. This theory has been accepted as the standard theory and is widely used to determine biophysical properties of specific bonds (Bartels et al. 2003; Björnham et al. 2009; Teulon et al. 2008; Thormann et al. 2006).

Distribution of rupture forces

The rupture probability density distribution (RPDD) function, $\rho(f)$, depends on the external force at the rupture event, f, the bond length, x_b, the thermal off-rate, k_{off}^{th}, the loading rate, r, and the thermodynamic energy unit, k_BT, where T is the absolute temperature and k_B is Boltzmann's constant (Husson and Pincet 2008),

$$\rho(f) = \frac{k_{off}^{th}}{r} e^{\frac{fx_b}{k_BT}} e^{-k_{off}^{th}\frac{k_BT}{rx_b}\left(e^{\frac{fx_b}{k_BT}}-1\right)}. \quad (1)$$

Here the loading rate, r, is the effective loading rate experienced by the bond. Any elastic components in a measurement system (e.g., elastic linkers connected to the molecules) have to be accounted for by the experimentalist to calculate the correct effective loading rate. Moreover, it is here assumed that no nonlinear effects are present, which means that the effective loading force increases linearly with time. Rupture forces for a specific bond under the influence of a linearly increasing force are, under ideal measurement conditions, random samples from the distribution function described by Eq. 1. A force frequency distribution can be created from a set of rupture forces, by means of histogram or density estimation, to which a fitting function is applied.

Frequency distributions—histogram and density estimator

Experimental data is collected into a frequency distribution from which the bond strength can be derived using a fitting function. Two common methods to compile the frequency distribution are histogram and kernel density estimation (KDE). In a classic histogram every data point is assigned

to one bin exclusively. The bin width and bin placement can be chosen arbitrarily. However, there are several theories that predict the optimal bin width to achieve best results (Hoaglin et al. 1983). It was later deduced that the bin width should be set to $3.49sn^{-1/3}$, where s is the estimate of the standard deviation (SD) and n is the number of samples (Scott 1979). Another method, which also scales the bin width with $n^{-1/3}$, is the Freedman-Diaconis rule (Freedman and Diaconis 1981), which is used in this work. It states that the bin width, Δx, should be

$$\Delta x = 2\frac{\mathrm{IQR}}{n^{1/3}}, \tag{2}$$

to achieve the best representation. Here IQR is the interquartile range, which is defined as the total length of the second and third quartile in a frequency distribution. This corresponds to the length of the interval along the force axis that divides the data points in such a way that 25% of the data is left on both sides. The IQR for an ensemble of an infinite number of measurements is directly given by the distribution function, Eq. 1. As an example of a typical distribution of rupture forces in a DFS experiment, the IQR amounts to $\sim$13 pN for a bond length of 5 Å. This value of IQR is virtually independent of the loading rate and the thermal off-rate but depends on the bond length in such a way that IQR, for instance, equals 22 and 9 pN for bond lengths of 3 and 7 Å, respectively. For 100 measurements and a bond length of 5 Å, the Freedman-Diaconis rule sets the bin width at $\sim$5.6 pN.

In contrast to the discretization in the classic histogram, KDE is a continuous representation with only one parameter to adjust. Every data point is replaced with a kernel, here chosen to be a normalized Gaussian function, centered at the data point with the width as the only degree of freedom. The sum of the Gaussian curves constitutes a continuous density estimate which is smooth in contrast to a classic discrete histogram. The width of the Gaussian curves has no, or very small, influence on the resulting fit of the rupture force density function, up to a certain limit of $\sim$10 pN (data omitted). The optimal width scales as $n^{-0.2}$ (Turlach 1993), which results in a width of 2.3 pN for a set of 100 measurements for a bond length of 5 Å. In the same way as for the classic histogram representation, the bond length sets this value, whereas the loading rate and the thermal off-rate have only minor influences.

Curve-fitting functions

In general there are two different options of fitting functions used in DFS: Gaussian (Bartels et al. 2007; Odorico et al. 2007b; Rico and Moy 2007; Strunz et al. 1999) and RPDD functions (Eq. 1) (Morfill et al. 2007; Neuert et al. 2006; Takeuchi et al. 2006; Tsukasaki et al. 2007). The choice of a Gaussian function is assumed to be based on the fact that it is a commonly used function in various fitting models and that it is easier to implement than an RPDD function. However, the RPDD function is favored by the fact that the theory of binding probability predicts this highly asymmetric distribution. The force that corresponds to the maximum value of the fitting function is referred to as the bond strength and is denoted by f^* in this work, see Fig. 1a.

Distribution, accuracy, and precision of the estimated bond strength

For a particular set of rupture forces (here denoted by subscript i), the error of the bond strength, ε_i, is defined as the difference between the bond strength obtained from the fitting procedure, f_i^*, and the true bond strength, f^*_{true},

$$\varepsilon_i = f_i^* - f^*_{\mathrm{true}}. \tag{3}$$

The true bond strength is defined as the inherent bond strength of the binding complex under the specific experimental conditions (temperature and loading rate). The central limit theorem states that a large set of mean values of independent random samples from a distribution of data can be approximated by a normal density distribution. The center value and the width of such a distribution describe the expected value and the variance of the mean values (Fig. 1b). The nonsymmetric distribution described by Eq. 1 and Fig. 1a has, in general, a mean value that is different from the maximum. However, it is shown (Tees 2001) that, although f^* is different from the mean value, the difference is virtually constant for the magnitude of variations in the parameters that can be expected for rupture experiments. This constant, relating the bond strength to the mean, is also independent of the loading rate for typical binding properties. This implies that the bond strengths and the mean values have the same normal distribution except for a constant shift along the force axis. In conclusion, the bond strengths obtained from the fitting procedure form a normal distribution and the distance from the center of this distribution to the true bond strength is the expected error, ε, of the bond strength (Fig. 1b). The expected error is also referred to as the accuracy. The SD of the distribution in Fig. 1b is a measure of the precision of the bond strength, which also can be seen as the reproducibility.

Evaluation of the bond length and the thermal off-rate

The bond strength, f^*, can be expressed (Evans and Ritchie 1997) as

$$f^* = \frac{k_{\mathrm{B}}T}{x_{\mathrm{b}}}\ln\left(\frac{rx_{\mathrm{b}}}{k_{\mathrm{off}}^{\mathrm{th}}k_{\mathrm{B}}T}\right). \tag{4}$$

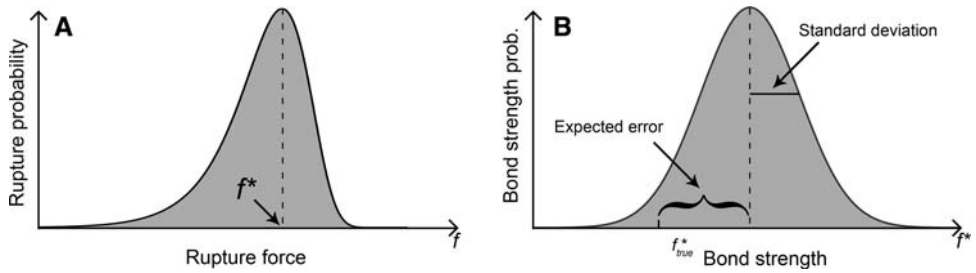

Fig. 1 **a** Schematic illustration of the RPDD for a single measurement. The peak corresponds to the bond strength, f^*, as indicated in the figure. **b** The measured bond strength follows a normal distribution, where the offset from the theoretical bond strength, f^*_{true}, is the expected error of the measurement. The precision of the bond strength is defined by the SD of the distribution

Normally in a DFS evaluation, the measured bond strengths are plotted versus the logarithm of the loading rates and, according to Eq. 4, a linear relation is expected. A linear fit is applied to calculate the bond length and the thermal off-rate. As a result of the central limit theorem, deviations from this straight line are normally distributed random errors, ε_i, with SD denoted by σ. Furthermore, the errors are assumed to have expectation values equal to zero and constant variances with respect to the loading rate, and to be independent of each other. These assumptions can normally be justified. In this study, we have verified these assumptions to be valid, by numerical simulations, for all parameter values used. This implies that the uncertainty of the parameters in the linear fit also follow a normal distribution (Mendenhall and Sincich 1995). The slope of the fit supplies the bond length, whereas the intersection point between the vertical axis and the interpolated fitting curve reveals the thermal off-rate. The uncertainty of these two parameters depends not only on the uncertainty of the bond strengths but also on the choice of experimental procedure such as the number of loading rates and their distribution within the chosen range.

The Gauss–Markov theorem states that, in a linear model, the best linear estimator is given by the least-squares line (Fox 1997). Thus, the best fit to the measured bond strengths is given by

$$\hat{f}^* = B_0 + B_1 \ln r, \tag{5}$$

where $\hat{f}^*$ is the bond strength of the least-squares line, and B_0 and B_1 are the fitting parameters, sometimes referred to as least-squares estimates. The least-squares line is defined as the line that has the lowest sum of squares of errors (SSE),

$$\text{SSE} = \sum_{i=1}^{m} \left[f_i^* - \hat{f}_i^*\right]^2 = \sum_{i=1}^{m} \left[f_i^* - (B_0 + B_1 \ln r_i)\right]^2, \tag{6}$$

where m is the number of different loading rates r_i. The SD of the slope of the least-squares line is given as

$$\sigma_{B_1} = \frac{\sigma}{\sqrt{\text{SS}_{rr}}}, \tag{7}$$

and the SD of B_0 is

$$\sigma_{B_0} = \sqrt{\frac{\sigma^2}{m}\left(\frac{\sum_{i=1}^{m} (\ln r_i)^2}{\text{SS}_{rr}}\right)} = \sigma_{B_1}\sqrt{\frac{1}{m}\sum_{i=1}^{m} (\ln r_i)^2}. \tag{8}$$

The quantity SS_{rr} depends only on the distribution of the loading rates and can be calculated as

$$\text{SS}_{rr} = \sum_{i=1}^{m} \left(\ln r_i - \overline{\ln r}\right)^2, \tag{9}$$

where $\overline{\ln r}$ is the mean value of the logarithms of the loading rates. The SDs of the fitting parameters, σ_{B_0} and σ_{B_1}, can be calculated from the information of the SD of the bond strengths and the distribution of the loading rates. Further details of linear fits and the uncertainties of the estimates can be found in textbooks (Mendenhall and Sincich 1995; Taylor 1997).

It is obvious from Eqs. 7–9 that the loading rates, on the logarithmic scale, should be chosen as far from the mean value as possible to minimize the SDs of the fit. In practice, this creates a dilemma since it is normally also of interest to examine the linearity of the slope, and a somewhat even distribution of the logarithms of the loading rates is therefore desired.

The slope of the least-squares line supplies the bond length as

$$x_\text{b} = \frac{k_\text{B}T}{B_1}. \tag{10}$$

Any error of B_1, referred to as σ_{B_1}, will propagate to the bond length and result in an error, σ_{x_b}, that is given as

$$\sigma_{x_\text{b}} = \left|\left(-\frac{k_\text{B}T}{B_1^2}\right)\sigma_{B_1}\right|. \tag{11}$$

Finally the propagation of error of the thermal off-rate, $\sigma_{k_\text{off}^\text{th}}$, is obtained from the relation

$$B_0 = \frac{k_\text{B}T}{x_\text{b}} \ln \frac{x_\text{b}}{k_\text{off}^\text{th} k_\text{B} T}, \tag{12}$$

from which the thermal off-rate can be extracted and its error derived as

$$\sigma_{k_{\text{off}}^{\text{th}}} = \left| \left(\frac{x_\text{b}}{k_\text{B}T} \right)^2 \text{e}^{-\frac{B_0 x_\text{b}}{k_\text{B}T}} \sigma_{B_0} \right|. \quad (13)$$

The errors of B_0 and B_1 are normally distributed, which implies that the errors of the bond length and thermal off-rate are also normally distributed.

The procedure described above establishes a framework to obtain the expected error and SD, which describe the accuracy and the precision, of the bond length and thermal off-rate. These parameters depend on the fitting results but also the choice of experimental setup with respect to the set of loading rates.

Simulation procedure

The simulation procedure models a DFS measurement procedure as closely as possible. We used loading rates in the interval 10^2–10^4 pN s^{-1} and assigned the values 5 Å and 10^{-3} s^{-1} to the bond length and the thermal off-rate, respectively. The latter two values, referred to as the true values, are similar to the reported experimental values for various single bonds (e.g., Berquand et al. 2005; Björnham et al. 2009; Merkel et al. 1999; Neuert et al. 2006; Schwesinger et al. 2000; Yuan et al. 2000). The temperature was set at 25°C as experiments are normally performed at room temperature. The first step in the procedure was to calculate the theoretical RPDD for a given loading rate, by means of Eq. 1. A number of stochastic rupture forces, obeying this probability distribution, were then computer-generated. A frequency distribution was constructed with the generated rupture forces, by means of histogram or KDE. The bond strength was calculated by fitting a function (a Gaussian or an RPDD) to the generated frequency distribution. The expectation value and variance of the bond strength are of interest and were calculated by repeating the simulation procedure a large number of times (10,000) to obtain a smooth and representative distribution of bond strengths. This distribution had a Gaussian shape as a consequence of the central limit theorem.

Simulation verification

An extraordinary careful simulation was initially performed to ensure that the simulation algorithm was legitimate and correct. For a loading rate of 100 pN s^{-1}, rupture force distributions each containing 10^9 measurements were generated, which rendered, by the use of KDE and RPDD, an expectation value for the bond strength of 77.3200 pN to compare with the theoretical value of 77.3202 pN. The difference of 0.2×10^{-3} pN verifies the validity of the simulation procedure.

Noise modeling method

Noise, of both electronic and mechanical nature, arises from all components in an experimental system. Examples of noise sources include fluctuations in laser intensity and profile, optical resolution, mechanical disturbances such as vibrations of components along the optical path, electrical noise produced by photodetectors, thermal vibrations, and amplifiers and other electronic devices. Moreover, noise can also arise from artefacts of the biological sample. The noise sources depend on the instrumentation and the technique used. Data processing can also introduce a certain amount of noise. The total noise in the system is an accumulated sum of several different noise sources, each with a possible unique amplitude and distribution. This sum can be expected to have an unknown nonconventional distribution. In this work we implemented and examined the influence of two common unbiased noise distributions: the normal and the uniform distribution, respectively. We applied the SD as a measure of the noise level in the case of normally distributed noise, whereas for the case of uniformly distributed noise the mean of the absolute values was used. Note that the mean of the absolute value of the normally distributed noise is $\sim$0.8 multiplied by the SD, which implies that applying a certain level of noise from the two dissimilar distributions results in a somewhat different amount of noise to the systems. However, since the distribution of noise is difficult or impossible for the experimentalist to control, it is the qualitatively influence induced by the noise that is of primary interest.

Frequency distributions of rupture forces from actual measurements are often found to be broader than predicted by the standard theory. An acknowledged explanation for the broadening is still lacking but can most likely be described as a combination of contributions originating from several different factors. Even though this issue has been addressed recently (Raible et al. 2006; Thormann et al. 2006), it is not clear how best to explain or model this phenomenon. In the model used in this work, two different noise distributions are applied which both generate a considerable broadening effect of the frequency distributions. This implies that we, in a phenomenological manner, have varying broadening of the frequency distributions that is realized by the introduction of noise and that the distributions are based on the standard theory.

Results and discussion

The results of the numerical simulations give quantitative information concerning the accuracy and precision of the extracted parameters which describe the uncertainty depending on the measurement procedure. We scrutinize the influence of frequency distribution method, fitting function, noise, and the choice of loading rates.

Frequency distributions

The comparison between the classic histogram and the KDE representation for creating a frequency distribution resulted in weak differences (<0.1 pN) of the bond strength (Fig. 2a). The results using the RPDD fitting function show that the KDE has lower variance, although the difference is significant only for a small number of measurements (<60). The expected error in the case with the histogram was slightly smaller (~0.05 pN for a large number of measurements) but also fluctuated as a result of bin placement for sets with few measurements. Note that the scale in Fig. 2a is significantly more detailed for the expected error than for the SD. For a larger number of measurements (>200), the accuracy and precision of the bond strength were practically similar for both methods. This fact holds for all levels of noise (data omitted), and the choice of method to create the frequency distribution was therefore found to have only limited influence on the resulting bond strength. However, the higher variance and instability of the classic histogram data (Fig. 2b) when the number of measurements is small (<100) can impact the interpretation and identification of multiple and nonspecific bindings, which suggests that KDE is the more reliable method. The oscillation of the expected error for the histogram data is caused by high sensitivity to the bin positions, i.e., the free choice of the position of the first bin.

Curve-fitting functions

In contrast to the similar behaviour of the two representations of the frequency distribution, the Gaussian and the RPDD fitting functions delivered results with significant differences. The most evident difference was that the Gaussian fitting function consistently returned a substantial expected error of the bond strength with a negative offset. Even under perfect conditions with several hundred noise-free measurements the expected bond strength obtained from fits with a Gaussian function underestimated the true bond strength by ~2.3 pN (Fig. 3a, dashed gray line). This significant error is a result of the fact that the RPDD has a highly nonsymmetrical shape along the force axis, with 64% of the cumulative rupture probability for forces below the true bond strength (Fig. 1a). As a result, the symmetric Gaussian function is centered at a force lower than the true bond strength. A great improvement was achieved when the RPDD function was applied. The expected error was close to zero even for a small number of measurements, and approached zero in the limit of an infinite number of measurements (Fig. 3a, dashed black line).

Noise-induced error

The actual distribution of noise in a measurement is often impossible to determine. Two commonly used functions to describe noise distributions are the uniform and normal distributions (Bryson et al. 2008; Cheng et al. 2005; McSharry and Smith 1999; Schuck 2000). These two distributions have different impact on the results, which arise from their interactions with the fitting functions. The expected error originating from all four combinations of fitting functions and noise distributions are plotted in Fig. 3b. It is evident that the choice of fitting function has a profound impact on the accuracy of the results. A very

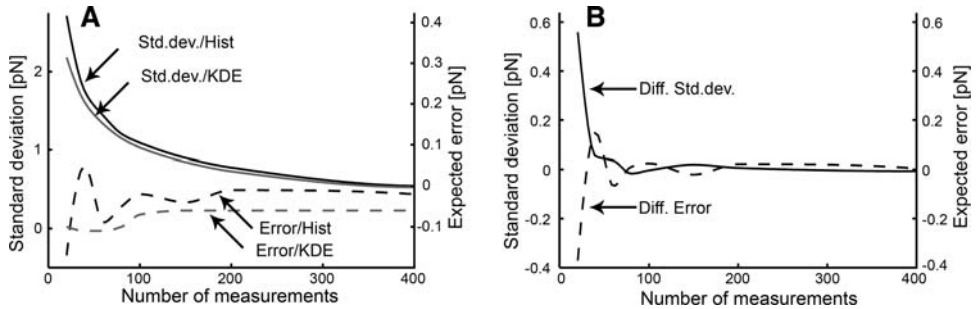

Fig. 2 **a** The *solid lines* show the SD of the bond strength distributions, whereas the *dashed lines* show the expected errors of the bond strengths. Black and gray lines refer to data from histogram and KDE representations, respectively. The SD and expected error of the bond strengths are nearly equal for the two methods of generating the frequency distribution. The KDE has a lower SD but an expected error that is slightly larger than for the classic histogram. For a small number of measurements the classic histogram representation is sensitive to bin placement. **b** Differences of the expected errors (*dashed line*) and of the SD (*solid line*) for two different placements of the bins (shifted by half the bin width) for the classic histogram representation when no noise is present. The instability for data sets with few points (<100) is evident. The RPDD is used as the fitting function for all points

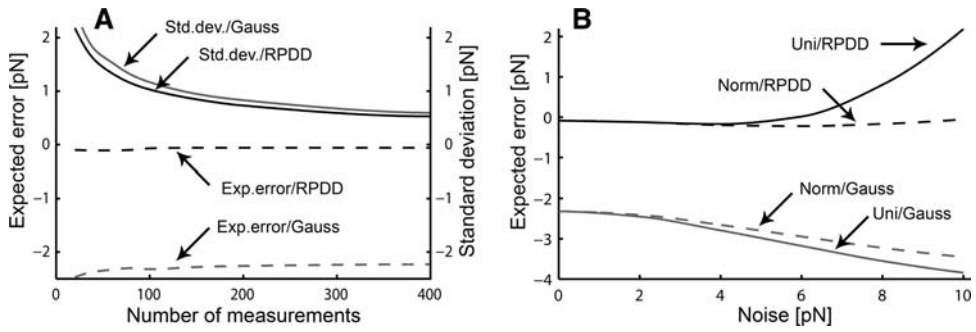

Fig. 3 **a** The expected error and SD of the bond strength for Gaussian and RPDD fitting functions, respectively, without noise in the system. *Solid* and *dashed lines* refer to the SD and the error of the expectation value of the bond strength, respectively. Black and gray lines refer to the RPDD and the Gaussian fitting functions, respectively. **b** The expected error of the bond strength as a function of the noise for all four combinations of fitting functions and noise distributions. *Solid* and *dashed lines* refer to uniformly and normally distributed noise, respectively. The *black lines* indicate RPDD and *gray lines* indicate Gaussian fitting functions. Results from the RPDD fits show high accuracy for both noise distributions up to 6 pN, after which the bond strengths become overestimated for uniformly distributed noise. Normally distributed noise has little effect on the expectation value of the bond strength. The obtained bond strength consequently underestimates the true bond strength when a Gaussian fitting function is used. In this case the noise distribution has little effect on the expected error, although uniformly distributed noise shifts the expectation value the most and induces the largest error. All values are taken as the mean values for the entire range of number of measurements

interesting observation is that normally distributed noise has virtually no impact on the expected error of the bond strength from an RPDD fit (Fig. 3b, dashed black line). This is in contrast to uniformly distributed noise that induces an expected error that increases strongly with noise level above 6 pN (Fig. 3b, solid black line). This phenomenon is explained by the fact that the extreme values of the applied uniform noise have different effects on the fitting procedure. Data points that are strongly displaced by the noise force the RPDD fit to higher values. This is caused by the fact that noise has a diffusive effect on the frequency distribution which means that rupture force data are effectively displaced in both positive and negative directions from the bond strength value. The RPDD is asymmetric in such a way that the rupture forces that are displaced in the positive force direction induce a larger error of the fit. This leads to a displacement of the fitting curve towards higher forces. This effect is more pronounced for the uniform distribution than for normally distributed noise since the probability for strong noise is higher in the former case.

Interestingly, the opposite effect is observed for the case with a Gaussian fitting function (Fig. 3b, solid and dashed gray lines). Notice that the error is significant even under a noise-free condition. The absolute error increases almost linearly with noise level for both the uniform and the normal noise distributions. The difference between the noise dependences of the two fitting functions is caused by noise-induced alterations of the rupture force frequency distribution curves. Even though the mean values of the frequency distribution curve remain unchanged, the alteration of the shape actuates the resulting bond strengths from the fits to drift in opposite directions.

The SD of the distribution of the bond strength from a fitting procedure describes the precision of the retrieved bond strength (Fig. 1b). The number of measurements, the noise level, and the noise distribution are parameters that influence the SD, as illustrated in Fig. 4a and b. It is apparent that the SD of the bond strength distribution is fairly stable for low levels of noise but increases strongly at higher noise levels. By comparison between Fig. 4a and b, we can also observe that uniformly distributed noise increases the SD more strongly than normally distributed noise. Therefore, uniformly distributed noise induces both higher expected errors (Fig. 3b) as well as higher SD than normally distributed noise.

The effect of the fitting function for three different noise levels (0, 6, and 10 pN) is illustrated in Fig. 5a and b. The RPDD function results in accurate bond strengths with acceptable variance in general, for both uniformly and normally distributed noise, but fails when the amplitude of the uniformly distributed noise exceeds 6 pN. In contrast, the bond strength generated from a Gaussian fitting function constantly underestimates the true bond strength. The probability distributions illustrated in Fig. 5a and b exhibit small variations between the case with uniformly and normally noise distribution, with the exception of high noise levels for the RPDD fitting function.

Accuracy and precision of the bond length and the thermal off-rate

Normally, an experiment is restricted to a certain interval of loading rates (r_{min}, r_{max}), due to both the instrumentation and practical limitations. The limiting factors can be the time to conduct the measurements and time-dependent

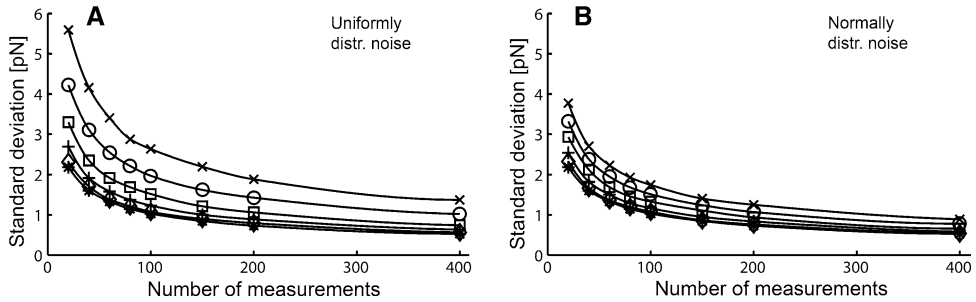

Fig. 4 SD of the bond strength distribution as a function of number of measurements for different noise levels in the system. **a** and **b** display data for uniformly and normally distributed noise, respectively. The noise levels are 0 (*asterisks*), 2 (*open diamond*), 4 (*plus*), 6 (*open square*), 8 (*open circle*), and 10 (*multiply*) pN. The RPDD fitting function has been used in all cases

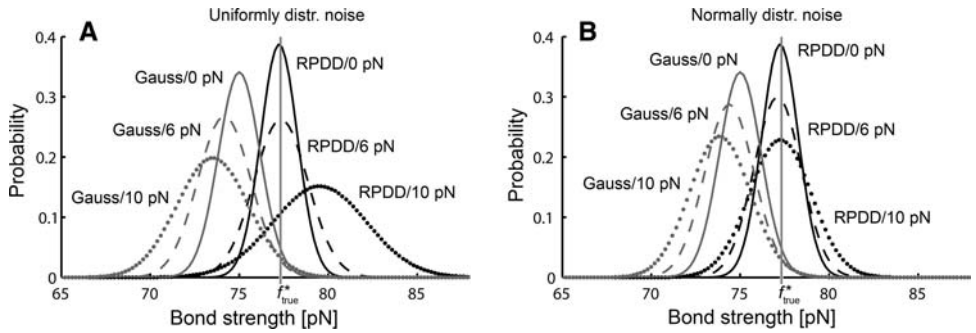

Fig. 5 Probability distribution for bond strength as a function of the fitting function and the noise level for sets of 100 measurements. *Black* and *gray lines* represent distributions with RPDD and Gaussian fitting functions, respectively. The accuracy and precision is studied for three different noise levels: 0 pN (*solid*), 6 pN (*dashed*), and 10 pN (*dotted*). The noise has uniform and normal distribution in **a** and **b**, respectively. If a Gaussian fitting function is used, the probability of acquiring the true bond strength is negligible. The *vertical gray line* marks the true bond strength value

alterations of the biological system. Furthermore, the total number of measurements, N, is a limiting factor, whereas the distribution of the m different loading rates r_i can be chosen arbitrarily within the allowed loading rate interval. An important issue to address is if the experimentalist should cover a large number of loading rates with only a few events each or a few loading rates with a large number of events each.

The applied noise discussed so far in this study is exclusively unbiased. However, it is also important to consider the case when a systematic error is present in only a part of the measurement data. For instance, consider the situation where an error in the calibration procedure of the force transducer occurs for one loading rate. This would result in a shift of the bond strength for that particular loading rate while the other bond strengths are unaffected. The resulting error from the fitting procedure is presented in Fig. 6a for the worst-case scenario when the forces at a limiting loading rate, here the lowest loading rate, suffer from a systematic error. The resulting error in thermal off-rate and bond length originating from this systematic error is substantial. The problem in this particular example could, in practice, be reduced by avoiding that any data point completely relies upon one particular calibration. Systematic errors can, in general, be eliminated or minimized by careful measurement procedures, which is in contrast to random noise that is inherent in the system (e.g., thermal vibrations). In the following we analyze the accuracy and precision of the thermal off-rate and the bond length in the case with unbiased random noise.

From the results presented hitherto, we conclude that the RPDD function applied on KDE provides the most accurate and reliable results, with a negligible expected error. Therefore, we used this combination exclusively in the following analysis. Measurements with different loading rates are, in practice, necessary to obtain the bond length and thermal off-rate by means of DFS. Our simulations demonstrate that the errors and SDs of the bond strengths are virtually independent of the loading rates, at least within the interval treated here. This means that the results showed above (for a loading rate of 100 pN s^{-1}) apply for the bond strengths at all relevant loading rates.

In this work, the SDs for the bond length and the thermal off-rate were assessed for a fixed number of $N = 1{,}000$ measurements, which is a reasonable number in practical situations. The measurements were partitioned into m loading rates in the interval 10^2–10^4 pN s^{-1}. For all cases, the upper and lower limits of loading rates were used, and

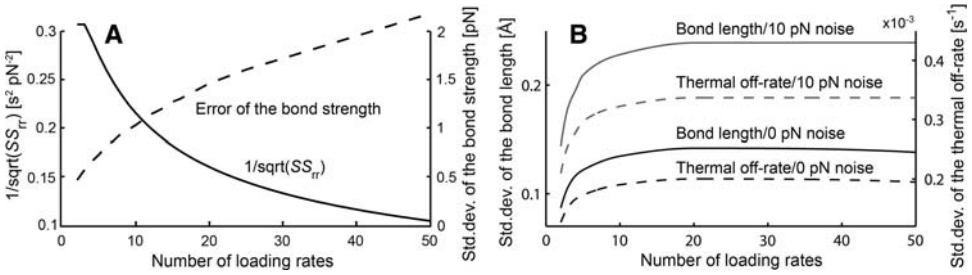

Fig. 6 **a** A systematic error, ε_{sys}, in all measurements at one particular loading rate introduces a substantial error. This error is suppressed by a large number of loading rates which therefore, in this context, is advantageous. The bond strength at the lowest loading rate has been assigned a constant additive force that represents the systematic error. The effect of this error is maximized since it has been applied to one of the limiting data points. A relative error of 1% corresponds to a systematic error of $\sim$0.77 pN in this case. **b** The two opposing factors for calculating the errors of the fitting parameter B_1. *Solid* and *dashed lines* refer to 1/sqrt(SS_{rr}) and the error of the bond strength, respectively. **c** The SD of the errors in bond length and thermal off-rate as a function of the number of different loading rates used under noise-free conditions (*black*) and 10 pN normally distributed noise (*gray*). *Solid* and *dashed lines* correspond to bond lengths and thermal off-rates, respectively. The best results, in presence of unbiased errors only, are obtained with few loading rates

the other $m - 2$ loading rates were chosen to be evenly distributed with respect to the logarithmic scale within the interval. We calculated the resulting precision of the bond length and thermal off-rate for various numbers of loading rates in the interval $2 \leq m \leq 50$.

Two opposing factors, the uncertainty of the calculated bond strength and the number of loading rates, govern the uncertainty of the bond length and thermal off-rate. The SS_{rr} factor increases with the number of loading rates, which decrease the uncertainty of the fit, see Eqs. 7–9. On the other hand, with a larger number of loading rates, the number of measurements for each point becomes smaller, which results in a higher uncertainty of the bond strength. The relation between these two factors, which is given by Eq. 7, determines how to choose the number of loading rates to achieve best precision. Figure 6b illustrates how the factors scale with the number of loading rates. The results displayed in Fig. 6c demonstrate that they virtually eliminate each other for large number of loading rates. However, the best results are achieved by focusing on the precision of the bond strengths. With only two loading rates used, the SD of the bond length and the thermal off-rate amounts to 0.087 Å and 0.13×10^{-3} s^{-1}, respectively, under noise-free conditions, and 0.14 Å and 0.21×10^{-3} s^{-1} with 10 pN amplitude of normally distributed noise.

The most evident change when a Gaussian fitting function is applied in lieu of an RPDD function is that all bond strengths are shifted towards lower forces, which is equivalent to introducing a consequent systematic error. This phenomenon does not influence the assessed bond length since it is calculated from the slope, although higher uncertainty of the Gaussian fit causes the SD of the bond length to increase by $\sim$15%. The thermal off-rate, on the other hand, is strongly affected. The true thermal off-rate of 1.0×10^{-3} s^{-1} is found to be 1.33×10^{-3} s^{-1}, with an SD that increases substantially, by a factor of 1.5.

The SD of both the bond length and the thermal off-rate scales linearly with the SD of the bond strengths, see Eqs. 7–13. The SD for any bond strength can be found from Fig. 3a for *N*/*m* measurements. This implies that an increase in the total number of measurements, for a given number of loading rates, will shift the SD of the bond strength according to the curve in Fig. 3a. This, in turn, has a linear impact on the resulting SD of the bond length and thermal off-rate. The qualitative dependence of the number of loading rates (Fig. 6c) therefore only has a minor effect by a change in *N*, i.e., the shape of the curves will remain nearly the same. The conclusion that the best precision is found with few loading rates thus holds regardless of the total number of measurements.

In conclusion, systematic and unbiased random errors have an opposite effect on the precision of the results. A large number of loading rates is less sensitive to occasionally systematic errors, whereas a small number of loading rates is favorable to minimize the effect of random unbiased noise and the stochastic nature of binding rupture forces themselves. If there is a reason to expect an occasional systematic error, the experimentalist has to consider the basic fact that fewer loading rates are preferable for better precision and weight this against the stabilizing effect of many loading rates as a consequence of the systematic error.

Conclusions

The distributions of error in the parameters commonly acquired by the standard method in DFS (bond strength, bond length, and thermal off-rate) were investigated in this study. This can serve as a guide for the experimentalist to estimate the uncertainty of the parameters acquired from DFS measurements. In conclusion, bond strengths retrieved

Table 1 Summary of the impact of different combinations of noise and methods on parameter accuracy and precision. The scale ranges from "−" to "+++," where the latter marks the best results. These marks serve as qualitative estimations of the accuracy and precision of the parameters and should not be interpreted as absolute grades

Error sources	Procedure/types		Accuracy and precision of the retrieved parameters		
			Bond strength	Bond length	Thermal off-rate
Frequency distribution	Classic histogram		−	−	−
	KDE		+	+	+
Fitting functions	RPDD		+++	+	+++
	Gaussian		−	−	−
Noise	Normally distributed	RPDD	+++	++	+++
		Gaussian	−	++	−
	Uniformly distributed	RPDD	++	−	++
		Gaussian	−	+	−
Number of loading rates	Few loading rates*		++	++	++
	Many loading rates*		−	−	−

* The total number of measurements is assumed to be constant, i.e., a small number of loading rates implies many measurements on each loading rate

when a Gaussian fit was applied to the frequency distributions of rupture force data are expected to underestimate the true value in all conditions addressed in this work. As a result, the thermal off-rate in such a DFS study can be expected to be strongly overestimated. In contrast, the results are far more accurate in the case with the RPDD function and this choice is strongly recommended. The RPDD fitting function is also, in the general case, less sensitive to noise than the Gaussian. Uniformly distributed noise has a more disturbing effect than normally distributed noise, and can even deteriorate the accuracy of the RPDD fitting function under heavy noise. Moreover, the introduction of noise into the modeling procedure can be considered as an approach to take into account different random variations (whose origins may be unknown) of the physical properties in an actual measurement. The variations induce, quite naturally, a significant broadening of the force distributions, and for this reason most experimental distributions are broader than expected by the standard theory. It is of high priority to establish the bond strengths with as high accuracy and precision as possible. Therefore, the number of different loading rates should be kept to a minimum to achieve best precision. The price to pay for this precision is a reduction of the number of investigated loading rates, which reduces the possibility to assess the linearity of the bond strength dependence on the logarithm of the loading rate. The resulting parameters also become more sensitive to occasional systematic error when the number of loading rates is small.

The "breakpoint" found in literature for the minimum number of measurements to obtain an acceptable precision of the bond strength is in general ~ 100. The slope of the SD curves, displayed in Fig. 3a, is a measure of the increase in precision as a function of N. We observe that the slope of the SD curves become shallower as N increases, which implies that the benefit, in terms of increasing precision, from each additional measurement decreases with N. The relative improvement of the precision of the bond length and thermal off-rate for one additional measurement is 0.84%, 0.48%, and 0.32% for $N = 50$, $N = 100$, and $N = 200$, respectively. However, since the slope is still relatively steep at $N = 100$ it is suggested that a greater number of measurements than 100 would be preferable as a lower limit.

Table 1 presents a qualitative concluding overview of the influences of the different factors in the DFS procedure. The impact of each procedure/type on the accuracy and precision of the three investigated parameters (bond strength, bond length, and thermal off-rate) is ranked with plus or minus symbols to indicate better and worse accuracy and precision, respectively. We conclude that the KDE and RPDD are the beneficial choices in DFS analysis.

Acknowledgment Economical support from the Magn. Bergvalls Foundation, Sweden, is gratefully acknowledged.

References

Arya M, Kolomeisky AB, Romo GM, Cruz MA, Lopez JA, Anvari B (2005) Dynamic force spectroscopy of glycoprotein Ib-IX and von Willebrand factor. Biophys J 88:4391–4401. doi:10.1529/biophysj.104.046318

Bartels FW, Baumgarth B, Anselmetti D, Ros R, Becker A (2003) Specific binding of the regulatory protein ExpG to promoter regions of the galactoglucan biosynthesis gene cluster of *Sinorhizobium meliloti*—a combined molecular biology and force spectroscopy investigation. J Struct Biol 143:145–152. doi:10.1016/S1047-8477(03)00127-8

Bartels FW, McIntosh M, Fuhrmann A, Metzendorf C, Plattner P, Sewald N, Anselmetti D, Ros R, Becker A (2007) Effector-stimulated single molecule protein–DNA interactions of a quorum-sensing system in *Sinorhizobium meliloti*. Biophys J 92:4391–4400. doi:10.1529/biophysj.106.082016

Bell MG (1978) Models for the specific adhesion of cells to cells. Science 200:618–627. doi:10.1126/science.347575

Berquand A, Xia N, Castner DG, Clare BH, Abbott NL, Dupres V, Adriaensen Y, Dufrene YF (2005) Antigen binding forces of single antilysozyme Fv fragments explored by atomic force microscopy. Langmuir 21:5517–5523. doi:10.1021/la050162e

Bianco P, Nagy A, Kengyel A, Szatmari D, Martonfalvi Z, Huber T, Kellermayer MSZ (2007) Interaction forces between F-actin and titin PEVK domain measured with optical tweezers. Biophys J 93:2102–2109. doi:10.1529/biophysj.107.106153

Björnham O, Bugaytsova J, Boren T, Schedin S (2009) Dynamic force spectroscopy of the Helicobacter pylori BabA–Lewis b Binding. Biophys Chem. doi:10.1016/j.bpc.2009.03.007

Bryson M, Tian F, Prestegard JH, Valafar H (2008) REDCRAFT: a tool for simultaneous characterization of protein backbone structure and motion from RDC data. J Magn Reson 191:322–334. doi:10.1016/j.jmr.2008.01.007

Chen W, Evans EA, McEver RP, Zhu C (2008) Monitoring receptor–ligand interactions between surfaces by thermal fluctuations. Biophys J 94:694–701. doi:10.1529/biophysj.107.117895

Cheng SW, Funke S, Golin M, Kumar P, Poon SH, Ramos E (2005) Curve reconstruction from noisy samples. Comput Geometry-Theory Appl 31:63–100. doi:10.1016/j.comgeo.2004.07.004

Derenyi I, Bartolo D, Ajdari A (2004) Effects of intermediate bound states in dynamic force spectroscopy. Biophys J 86:1263–1269. doi:10.1016/S0006-3495(04)74200-9

Evans E (1999) Looking inside molecular bonds at biological interfaces with dynamic force spectroscopy. Biophys Chem 82:83–97. doi:10.1016/S0301-4622(99)00108-8

Evans E, Ritchie K (1997) Dynamic strength of molecular adhesion bonds. Biophys J 72:1541–1555. doi:10.1016/S0006-3495(97)78802-7

Fox J (1997) Applied regression analysis, linear models, and related methods. SAGE, Thousand Oaks

Freedman D, Diaconis P (1981) On the maximum deviation between the histogram and the underlying density. Z Wahrscheinlichkeitstheorie Verwandte Geb 58:139–167. doi:10.1007/BF00531558

Fuhrmann A, Anselmetti D, Ros R, Getfert S, Reimann P (2008) Refined procedure of evaluating experimental single-molecule force spectroscopy data. Phys Rev E Stat Nonlin Soft Matter Phys 77 (3.1):031912

Hoaglin DC, Mosteller F, Tukey JW (1983) Understanding robust and exploratory data analysis. John Wiley & Sons, New York

Husson J, Pincet F (2008) Analyzing single-bond experiments: Influence of the shape of the energy landscape and universal law between the width, depth, and force spectrum of the bond. Phys Rev E Stat Nonlin Soft Matter Phys 77 (3.2):026108

Kramers HA (1940) Brownian motion in a field of force and the diffusion model of chemical reactions. Physica 7:284–304. doi:10.1016/S0031-8914(40)90098-2

Lee CK, Wang YM, Huang LS, Lin SM (2007) Atomic force microscopy: determination of unbinding force, off rate and energy barrier for protein–ligand interaction. Micron 38:446–461. doi:10.1016/j.micron.2006.06.014

Marshall BT, Sarangapani KK, Lou JH, McEver RP, Zhu C (2005) Force history dependence of receptor–ligand dissociation. Biophys J 88:1458–1466. doi:10.1529/biophysj.104.050567

McSharry PE, Smith LA (1999) Better nonlinear models from noisy data: attractors with maximum likelihood. Phys Rev Lett 83:4285–4288. doi:10.1103/PhysRevLett.83.4285

Mendenhall W, Sincich T (1995) Statistics for engineering and the sciences, 4th edn. Prentice-Hall International, Inc., Englewwod Cliffs

Merkel R, Nassoy P, Leung A, Ritchie K, Evans E (1999) Energy landscapes of receptor–ligand bonds explored with dynamic force spectroscopy. Nature 397:50–53. doi:10.1038/16219

Morfill J, Blank K, Zahnd C, Luginbuhl B, Kuhner F, Gottschalk KE, Pluckthun A, Gaub HE (2007) Affinity-matured recombinant antibody fragments analyzed by single-molecule force spectroscopy. Biophys J 93:3583–3590. doi:10.1529/biophysj.107.112532

Neuert G, Albrecht C, Pamir E, Gaub HE (2006) Dynamic force spectroscopy of the digoxigenin–antibody complex. FEBS Lett 580:505–509. doi:10.1016/j.febslet.2005.12.052

Odorico M, Teulon JM, Berthoumieu O, Chen SWW, Parot P, Pellequer JL (2007a) An integrated methodology for data processing in dynamic force spectroscopy of ligand–receptor binding. Ultramicroscopy 107:887–894. doi:10.1016/j.ultramic.2007.04.019

Odorico M, Teulon JM, Bessou T, Vidaud C, Bellanger L, Chen SWW, Quemeneur E, Parot P, Pellequer JL (2007b) Energy landscape of chelated uranyl: antibody interactions by dynamic force spectroscopy. Biophys J 93:645–654. doi:10.1529/biophysj.106.098129

Perret E, Leung A, Feracci H, Evans E (2004) Trans-bonded pairs of E-cadherin exhibit a remarkable hierarchy of mechanical strengths. Proc Natl Acad Sci USA 101:16472–16477. doi:10.1073/pnas.0402085101

Raible M, Evstigneev M, Bartels FW, Eckel R, Nguyen-Duong M, Merkel R, Ros R, Anselmetti D, Reimann P (2006) Theoretical analysis of single-molecule force spectroscopy experiments: heterogeneity of chemical bonds. Biophys J 90:3851–3864. doi:10.1529/biophysj.105.077099

Rico F, Moy VT (2007) Energy landscape roughness of the streptavidin–biotin interaction. J Mol Recognit 20:495–501. doi:10.1002/jmr.841

Schuck P (2000) Size-distribution analysis of macromolecules by sedimentation velocity ultracentrifugation and Lamm equation modeling. Biophys J 78:1606–1619. doi:10.1016/S0006-3495(00)76713-0

Schwesinger F, Ros R, Strunz T, Anselmetti D, Guntherodt HJ, Honegger A, Jermutus L, Tiefenauer L, Pluckthun A (2000) Unbinding forces of single antibody-antigen complexes correlate with their thermal dissociation rates. Proc Natl Acad Sci USA 97:9972–9977. doi:10.1073/pnas.97.18.9972

Scott DW (1979) On optimal and data-based histograms. Biometrika 66:605–610. doi:10.1093/biomet/66.3.605

Strunz T, Oroszlan K, Schafer R, Guntherodt HJ (1999) Dynamic force spectroscopy of single DNA molecules. Proc Natl Acad Sci USA 96:11277–11282. doi:10.1073/pnas.96.20.11277

Takeuchi O, Miyakoshi T, Taninaka A, Tanaka K, Cho D, Fujita M, Yasuda S, Jarvis SP, Shigekawa H (2006) Dynamic-force spectroscopy measurement with precise force control using atomic-force microscopy probe. J Appl Phys 100:074315

Taylor JR (1997) An introduction to error analysis : the study of the uncertainties in physical measurements, 2nd edn. University Science, Sausalito

Tees D (2001) Reliability theory for receptor–ligand bond dissociation. J Chem Phys 114:7483–7496. doi:10.1063/1.1356030

Teulon JM, Parot P, Odorico M, Pellequer JL (2008) Deciphering the energy landscape of the interaction uranyl–DCP with antibodies using dynamic force spectroscopy. Biophys J 95:L63–L65. doi:10.1529/biophysj.108.141937

Thormann E, Hansen PL, Simonsen AC, Mouritsen OG (2006) Dynamic force spectroscopy on soft molecular systems: improved analysis of unbinding spectra with varying linker

compliance. Colloids Surf B Biointerfaces 53:149–156. doi:10.1016/j.colsurfb.2006.08.015

Touhami A, Jericho MH, Beveridge TJ (2007) Molecular recognition forces between immunoglobulin G and a surface protein adhesin on living *Staphylococcus aureus*. Langmuir 23:2755–2760. doi:10.1021/la0628930

Tsukasaki Y, Kitamura K, Shimizu K, Iwane AH, Takai Y, Yanagida T (2007) Role of multiple bonds between the single cell adhesion molecules, nectin and cadherin, revealed by high sensitive force measurements. J Mol Biol 367:996–1006. doi:10.1016/j.jmb.2006.12.022

Turlach BA (1993) Bandwidth selection in kernel density estimation: a review. Discussion paper 9307

Williams PM (2003) Analytical descriptions of dynamic force spectroscopy: behaviour of multiple connections. Anal Chim Acta 479:107–115. doi:10.1016/S0003-2670(02)01569-6

Yuan CB, Chen A, Kolb P, Moy VT (2000) Energy landscape of streptavidin–biotin complexes measured by atomic force microscopy. Biochemistry 39:10219–10223. doi:10.1021/bi992715o

Zhang XH, Bogorin DF, Moy VT (2004) Molecular basis of the dynamic strength of the sialyl Lewis X–selectin interaction. ChemPhysChem 5:175–182. doi:10.1002/cphc.200300813